Supporting Information (SI)

Engineering Shelf-Stable Coating for Microfluidic Organ-on-a-Chip using Bioinspired Catecholamine Polymers

Sultan Khetani [a,b,c], Kar Wey Yong[#a,b,d], Vinayaraj Ozhukil Kollath[#e], Erin Eastick[a,b], Milad Azarmanesh[a,b], Kunal Karan[e], Arindom Sen[b,c,d,e], Amir Sanati Nezhad*[a,b,c]

[a] *BioMEMS and Bioinspired Microfluidic Laboratory, Department of Mechanical and Manufacturing Engineering, University of Calgary, Calgary, Alberta T2N 1N4, Canada*
[b] *Center for Bioengineering Research and Education, Schulich School of Engineering, University of Calgary, Calgary, Alberta T2N 1N4, Canada*
[c] *Biomedical Engineering Graduate Program, University of Calgary, Calgary, Alberta T2N 1N4, Canada*
[d] *Pharmaceutical Production Research Facility, Schulich School of Engineering, University of Calgary, Alberta T2N 1N4, Canada*
[e] *Department of Chemical and Petroleum Engineering, University of Calgary, Calgary, Alberta T2N 1N4, Canada*

∗Corresponding author at: Department of Mechanical and Manufacturing Engineering, 2500 University Drive NW, Calgary, Alberta, Canada T2N 1N4

E-mail address: amir.sanatinezhad@ucalgary.ca ;

Table S1. Organ on chip (OOC) products

Below is the list of key companies with OOC products or chips. Most of the companies supply PDMS fluidic layers of various designs, tubes for connecting the channels with the source of media and reagents, and protocols for chip bonding, cleaning and coating with chemical or polymer materials. Although their materials are supplied in sophisticated packaging, none of these companies offer sterile, precoated chips with long shelf-life at room temperature.

Company	Product	Microchannel coating	Longevity	Storage
Emulate	Liver-chip, Lung-chip, Intestine-chip, proximal Tubule Kidney-chip	ECM coating	-	4°C, and 20°C
Aim biotech	3D culture chips	ECM coating	-	Not given
SynVivo	SynBBB - Blood Brain Barrier model SynTumor - Cancer models, SynRAM - Inflammation model, SynTox (Toxicology)	-	6 months (uncoated pdms chip)	Room temperature
Mimetas	Organo plates	ECM coating	-	-
Tissuse	HUMIMIC Chip2 HUMIMIC Chip3 HUMIMIC Chip4 HUMIMIC Chip XX/XY	-	-	-
Hesperso	Only chips	-	-	-
Alveolix	PDMS chips	-	-	-
Eht technologies	24-well format Silicone rack	-	-	-
Xonachips	2-Compartment (SND), 3-Compartment (TCND), Round (RD), 2-Compartment (XC) 3-Compartment (XC-T)	XC Pre-coat™, Poly-d-lysine solution	-	-
Axosim	PDMS chips	-	-	-

SI2. Simulating the flow of polymers and media within the microchannel

Numerical simulations were performed with Gerris open source code to first study the effect of shear stress on controlling the thickness of the coated polymers within the microchannels [1-2]. The physical parameters assigned to the simulations were set to be similar to the experimental conditions. The simulation data provides details about the shear stress on the wall of the microchannel as a result of the flow of polymer precursors and cell culture media. The viscosity and density of the polymers being nearly the same as water. The flow of water into the channel was simulated at different velocity magnitudes of 15 µL min^{-1}, 30 µL min^{-1}, 60 µL min^{-1}, 90 µL min^{-1} and 120 µL min^{-1} for analyzing the shear stress near the channel walls (**Figure S1 A)**. The data were then used to identify the optimal flow rate for coating the microchannels (**Figure S1 A (inset)**).

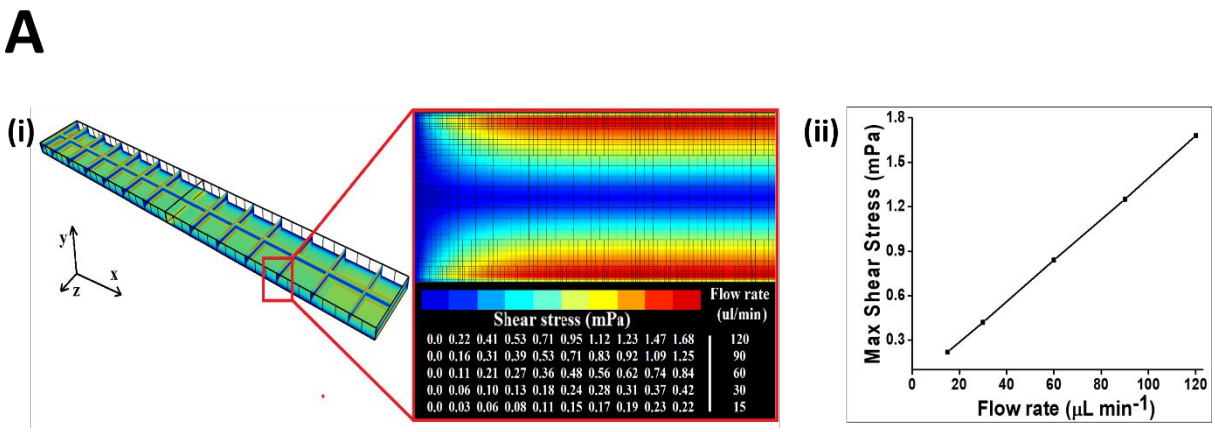

Figure S1 A(i) Shear stress due to the injection of Polydopamine (PDA) and Polynorepinephrine (PNE) precursors in the microchannel at 15 µL min^{-1}, 30 µL min^{-1}, 60 µL min^{-1}, 90 µL min^{-1} and 120 µL min^{-1} flow rates. (**ii**) Maximum shear stress experienced at the microchannel walls due to the fluid flow. At 120 µL min^{-1}, microchannel walls experienced the highest shear stress of 1.68 MPa.

The simulation of fluid flow within the microchannels was also used for minimizing the effect of shear stress resulting from the flow of culture media over cells cultured within the chip. For simulating the effect of shear stress of culture media on the cells, the microchannel was filled with air, and a water drop was introduced to the main channel at the inlet reservoir to replace the air. Considering the gravity propelled force, the water paves all the way through the microchannel. The contact angle of water-air-walls was adjusted to mimic different conditions of surface coating for both PDA and PNE [3].

The governing equations are based on conservation equations for incompressible, variable-density flow with surface tension and gravity terms (equation S1). Besides, the advection equation for the fluid density is used in vector form as shown in equations S1-S4 [2, 4].

$$\rho(\partial_t \boldsymbol{u} + \boldsymbol{u}.\nabla\boldsymbol{u}) = -\nabla p + \nabla.(2\mu\boldsymbol{D}) + \sigma\kappa\delta_s\boldsymbol{n} + \rho\boldsymbol{g}, \quad \text{(S1)}$$

$$\partial_t \rho + \nabla.(\rho\boldsymbol{u}) = 0, \quad \text{(S2)}$$

$$\nabla.\boldsymbol{u} = 0, \quad \text{(S3)}$$

$$\partial_t c + \nabla.(c\boldsymbol{u}) = 0, \tag{S4}$$

where $\boldsymbol{u} = (u, v, w)$ denotes velocity vector, p is pressure, $\mu(\boldsymbol{x}, t)$ is dynamic viscosity, $\boldsymbol{g}$ is gravity acceleration, $\rho(\boldsymbol{x}, t)$ is fluid density, and $\boldsymbol{D}$ is deformation tensor $\left(D_{ij} = \left(\partial_i u_j + \partial_j u_i\right)/2\right)$. δ_s as the Dirac delta function confirms that surface tension coefficient **(σ)** is clarified on the interface. k denotes curvature radius of the interface and $\boldsymbol{n}$ defines unit outward vector, perpendicular to the interface [1, 5-6].

The volume of fluid (VOF) method was used to simulate the water-air interface. A VOF function $c(\boldsymbol{x}, t)$ was used to introduce volume fraction of the water in each cell of the computational mesh. The geometrical VOF advects the volume fraction field for all computational cells inside the channel [2]. The viscosity and density were defined in the code as equations S5 and S6, respectively.

$$\mu = c\mu_w + (1 - c)\mu_a, \tag{S5}$$

$$\rho = c\rho_w + (1 - c)\rho_a, \tag{S6}$$

where subscripts *w* and *a* are the water and air, respectively [4]. A piecewise-linear VOF scheme was used to separate phases from each other and reconstruct the interface of water-air [2, 5, 7-8]. The interface in each cell was represented by a plane presented in equation (S7) [2].

$$\boldsymbol{m}.\boldsymbol{x} = \alpha, \tag{S7}$$

where $\boldsymbol{x}$ is position vector and $\boldsymbol{m}$ is vector locally normal to the interface. The parameter α was then defined assuming that the fluid volume maintained within the cell is equal to c. The detailed description is provided somewhere else [1-2].

Finite volume method (FVM) discretization was used to solve the considered governing equations. The volume fraction/density and pressure was modeled with the second-order staggered temporal discretization was used to model [2]. The Crank–Nicholson scheme was applied to discretize the viscous terms. All variables were collocated as volume-averaged at the center of each discretized volume mesh. The discretized momentum equation was re-organized to a Helmholtz-type and solved by an improved multi-level Poisson solver in order to improve numerical efficiency. The combination of a balanced-force surface tension discretization and a height-function curvature estimation was used to decrease problematic parasitic currents arising from the original Continuum-Surface-Force approach [8]. The three-dimensional water-air-solid contact angle algorithm was implemented in the code similar to the previously reported work [3, 9]. For the boundary conditions, the microchannel walls have a slip condition based on the defined water-air contact angles obtained on the PDA and PNE coated surfaces (**Figure 2E**). The inlet was set to Neumann boundary condition for water velocity at the top and outflow boundary for the outlet of the microchannel. The outlet was set to an outflow condition that allowed the flow to smoothly get out of the microchannel until the water fills the entire microchannel. The height of the inlet microchannel was set to 5 mm with a hydraulic diameter of 1.2 mm. Considering the rest of the microchannel geometry was filled with the air, the initial condition was set as to when the water slightly filled the microchannel (for the height of 100 μm from the top). The result showed that the different contact angles change the maximum liquid velocity at the middle of the microchannel as well as next to the walls (**Figure S1 B**). The resulting shear stress on the

microchannel is least, 1.10 MPa and 1.14 MPa for both PDA and PNE, for the most hydrophilic surface coatings obtained for 120 µL min^{-1}.

Based on the simulation results, it can be inferred that higher coating flow rates offer better surface coatings in comparison with low coating flow rates. Which in turns creates highly hydrophilic surface offering low shear stress due to the cell media

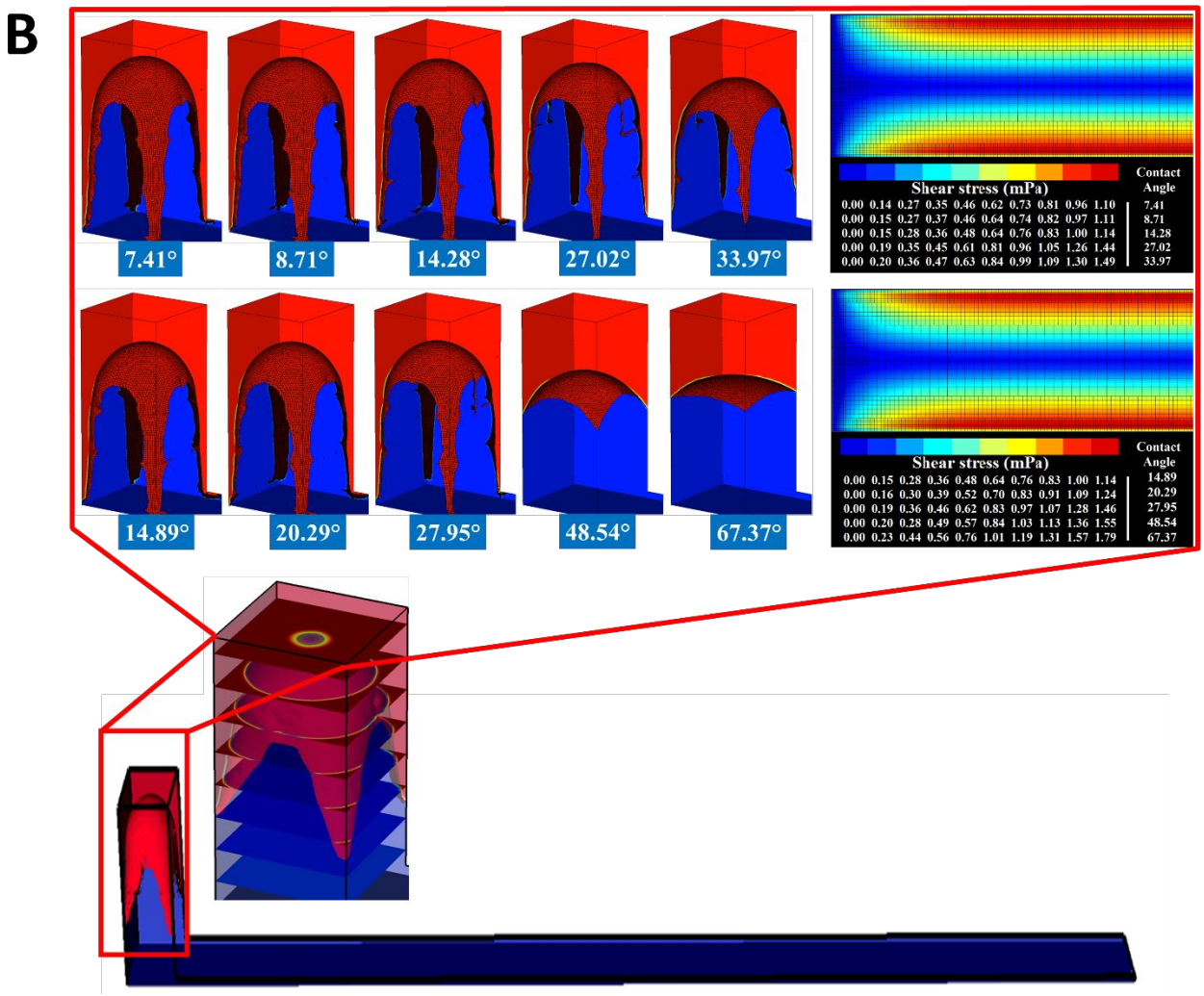

Figure S1 B. Simulation of culture media flow profile from the reservoir to the microchannel coated with PDA and PNE with 15 µL min^{-1}, 30 µL min^{-1}, 60 µL min^{-1}, 90 µL min^{-1} and 120 µL min^{-1} flow rates. Shear stress due to cell media flowing from the reservoir is least, 1.10 MPa in PDA and 1.14 MPa in PNE, for chips coated at 120 µL min^{-1} flow rate.

SI3. Flow coated PDA and PNE substrates improve cell adhesion and proliferation

The highly hydrophobic pristine PDMS surface is known to limit cell adhesion and proliferation. In this study, the single-step coating of the PDMS surface with either PDA or PNE improved the adhesion of CAD cells by more than 10 folds ($p < 0.05$) compared to that of the pristine PDMS surface (**Figure S2 A**). Interestingly, the flow-based PNE coating technique resulted in a higher cell adhesion ($p < 0.05$) than the static-based PNE coating technique. However, no significant difference ($p > 0.05$) was detected for cell adhesion when comparing the flow-based PDA coatings with the static-based technique (**Figure S2 A**). Alamar Blue proliferation assay showed an increased CAD cell population in both the flow-based PNE and PDA coating techniques while there was a decrease in the CAD cell population in the pristine PDMS and static-based PNE and PDA coating techniques (**Figure S2 B**). A previous study demonstrated that the coating of PDMS surfaces with PDA without ECM using a static-based coating technique enhances cell adhesion but decreases cell proliferation [10]. Our developed flow-based polycatecholamine coating technique is not only able to improve cell adhesion but also increases cell proliferation.'

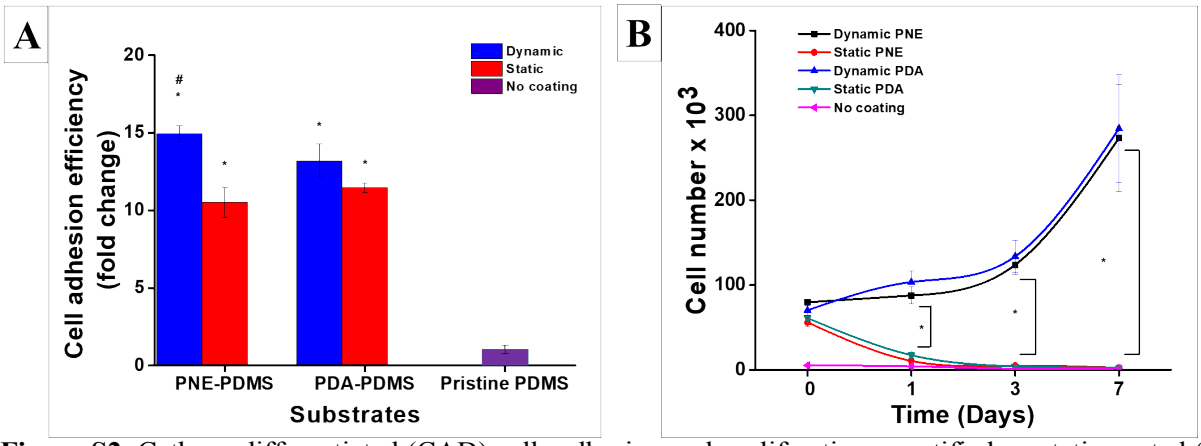

Figure S2. Cath. -a-differentiated (CAD) cells adhesion and proliferation quantified on static coated (120 min) and dynamically coated (120 µl min^{-1} for 120 min) Polydimethylsiloxane (PDMS) with PNE and PDA, and pristine PDMS substrates. (A) Flow-coated PDMS showed significantly higher cell adhesion for PNE coating compared to that static coated substrates. Although high in cell adhesion, flow-coated PDA substrate did not show any significant difference compared to the static coating. # indicates $p < 0.05$ relative to static-based PNE coating technique and * indicates $p < 0.05$ relative to pristine PDMS. (B) Cell population (represented cell proliferation) increased for both PNE and PDA flow-coated substrates while decreased on pristine PDMS, static-based PNE, and PDA coating technique groups. * indicates $p < 0.05$.

SI4. Effect of PDA and PNE coatings on the transparency of the chips

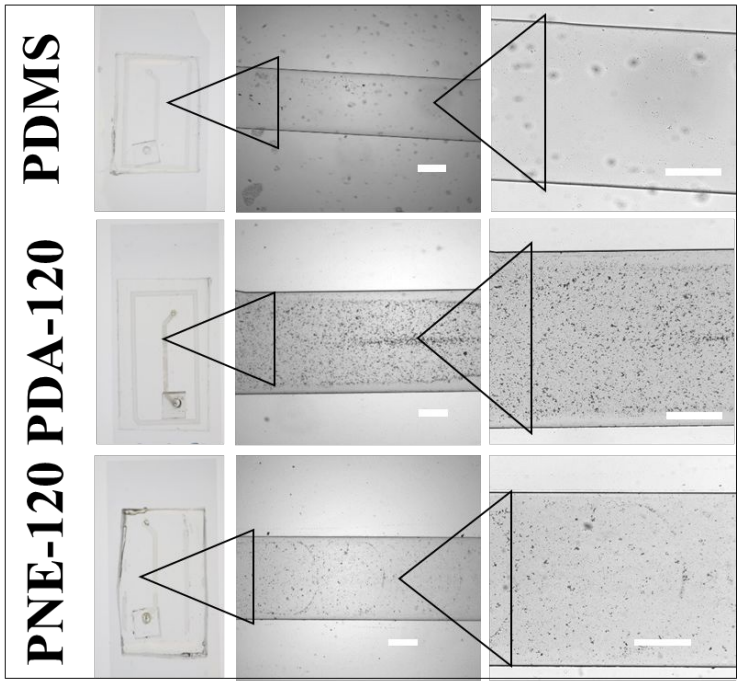

Figure S3. The transparency of the microfluidic chips coated with PDA and PNE at 120 μL min^{-1} for 120 min (scale bar: 2 mm).

SI5. Contact angle measurements

Images of water contact angle data presented in **Figure 2B** are given below in **Figure S4**. The contact angle of the glass substrate was measured to be 61.22°. Spin-coating PDMS turned the surface hydrophobic and increased the contact angle to 109.28°. PDMS modified with PDA and PNE turned to hydrophilic within 15 min of coating compared to the unmodified PDMS. At the end of 120 min of the polymer coating, the contact angles of PDA- and PNE-modified PDMS surfaces were measured to be 7.41° and 14.89°, respectively.

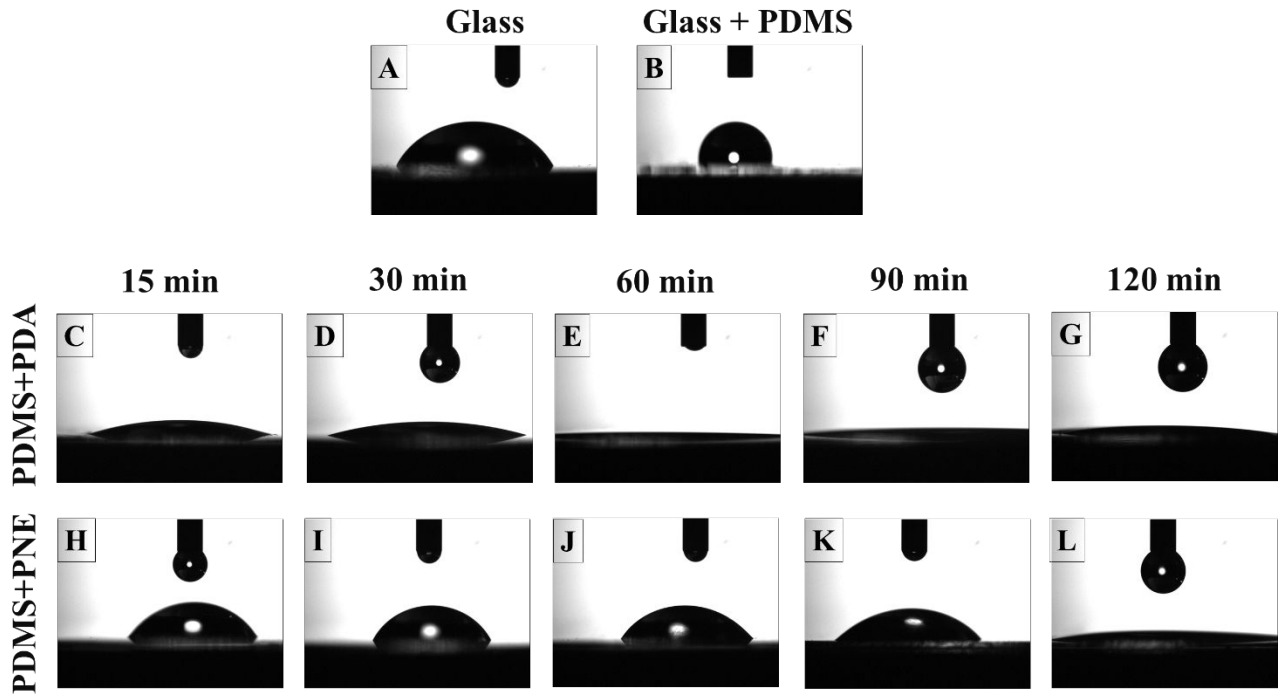

Figure S4. Contact angles of the glass substrate and polymer modified surfaces. (**A**) Glass, (**B**) Polydimethylsiloxane (PDMS) -coated glass substrate, (**C-G**) PDMS surface coated with PDA for 15 min to 120 min, and (**H-L**) PDMS surface coated with PNE from 15 min to 120 min.

SI6. MALDI-ToF-MS control peaks

Table S2. The baseline peaks of the MALDI-matrix, monomers, polymers and the test media are given in the table below.

Compound	Peaks	Reference
MALDI matrix	HCCA+H = 190.05, HCCA+Na = 212.03, NCCA+K = 238.005, 2HCCA+H = 379.09, 2HCCA+Na = 401.07, 2HCCA+K = 417.04, Acetalidine + H = 136.07, Acetalidine + Na =158 05, Acetalidine + K = 174.03	
Tris buffer	122	[11]
DA	154.4	
PDA	402.2	
NE	169. 07	[12]
PNE	292	
Trypsin	805.9, 907.1, 1112.3, 1154.3, 1434.7, 2164.3, and 2274.6	
PEI	104.11, 147.15, 190.19, 233.23, 276.27, 319.31, 362.35, 405.39, 448.43	[13]

With the objective to identify traces of the polymers in different test media collected from the microfluidic chips, baseline signals of DMEM cell media, PBS, tris buffer, trypsin, dopamine and norepinephrine monomers, polydopamine and polynorepinephrine and polyethyleneimine were obtained using MALDI-ToF MS analysis (**Figure S5**). These signals were used for comparing the signals obtained from polymer coated chips when tested in the presence of PBS, ethanol, cell media, and trypsin.

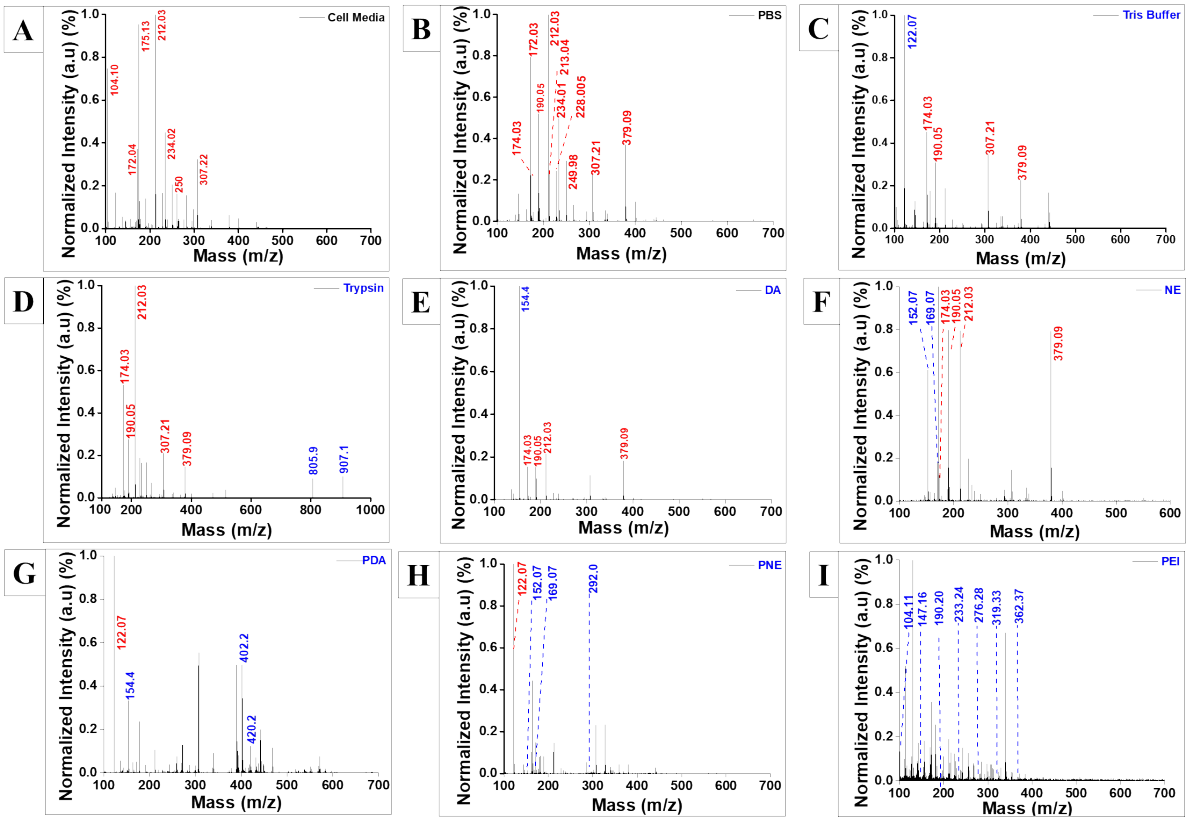

Figure S5. Matrix-Assisted Laser Desorption Ionization Time-of-Flight Mass Spectrometry (MALDI-ToF-MS) baseline spectra. (**A**) Cell media, (**B**) Phosphate-buffered saline (PBS), (**C**) Tris buffer, (**D**) Trypsin, (**E**) Dopamine hydrochloride, (**F**) Norepinephrine hydrochloride, (**G**) Polydopamine (PDA), (**H**) Polynorepinephrine (PNE) and (**I**) Polyethyleneimine (PEI).

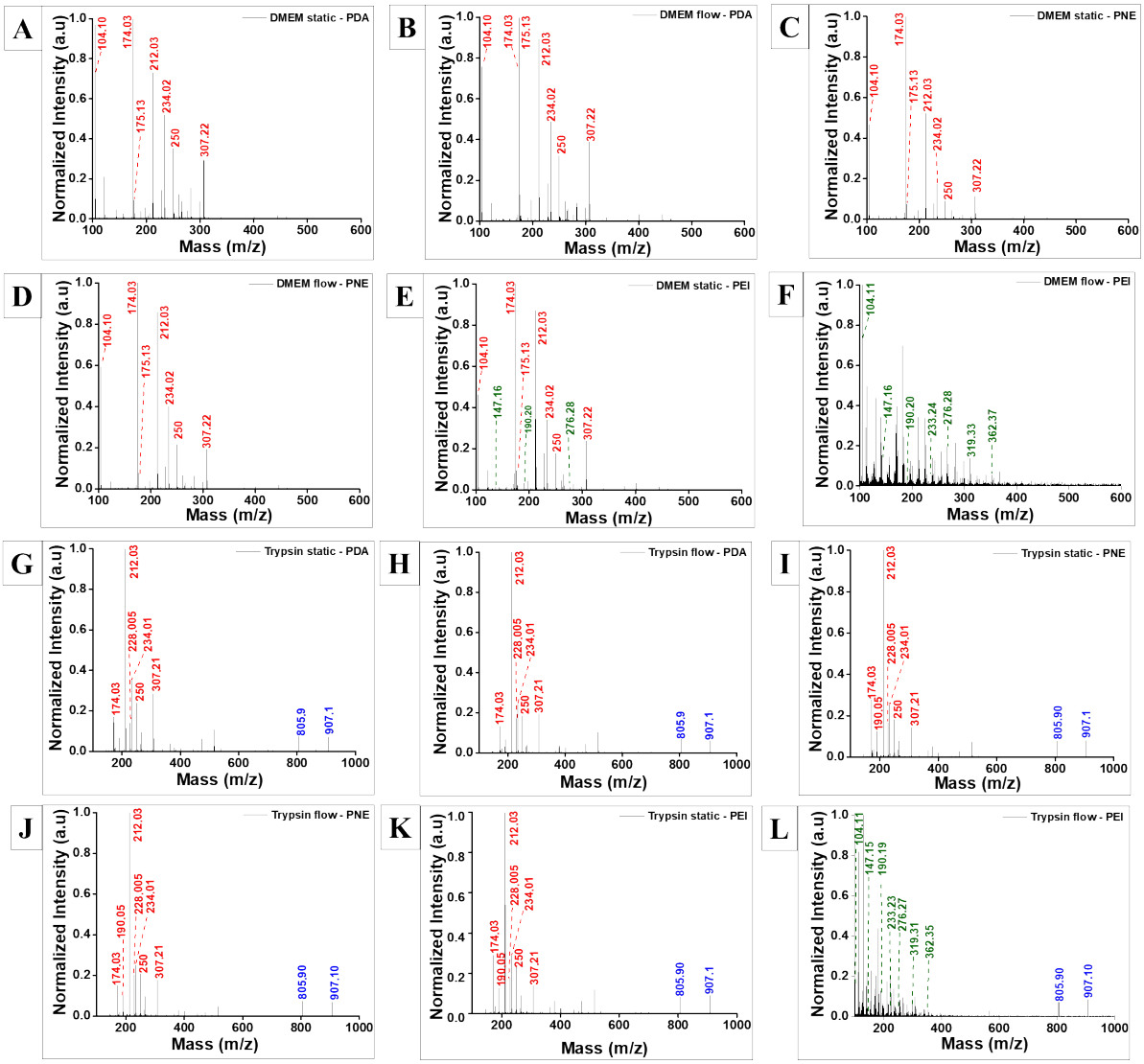

Figure S6. MALDI-ToF MS analysis of the media collected from the microfluidic chips treated with cell media, where the microchannels are treated with (**A**) PDA at static condition, (**B**) PDA under continuous flow, (**C**) PNE at static condition, (**D**) PNE under continuous flow, (**E**) PEI at static condition, and (**F**) PEI. MALDI-ToF MS analysis of the microfluidic chips subject to trypsin for (**G**) PDA coated at static condition, (**H**) PDA under continuous flow, (**I**) PNE at static condition, (**J**) PNE under continuous flow, (**K**) PEI at static condition, and (**L**) PEI under continuous flow.

SI7. Cell viability analysis

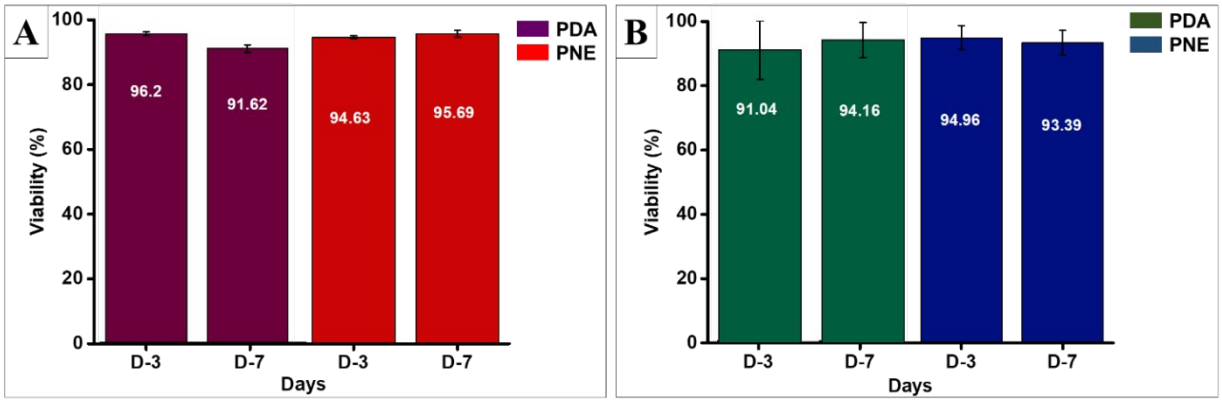

Figure S7. On-chip cell viability on day-3 and day-7 for microfluidic chips coated with PDA and PNE. (**A**) CAD cells and (**B**) hCMEC/D3 cells. All data points represent an average of 3 measurements (n=3), and the error bar is the standard error of the mean. ($p > 0.05$)

SI8. Storage of microfluidic chips at room temperature

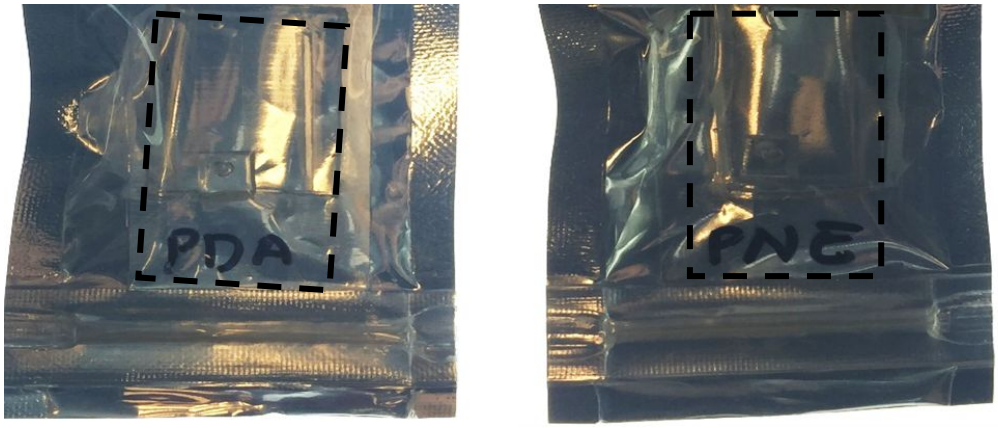

Figure S8. PDA and PNE coated microfluidic chips were packed and stored in sealable plastic bags at room temperature.

SI9. Alamar blue assay standard curve

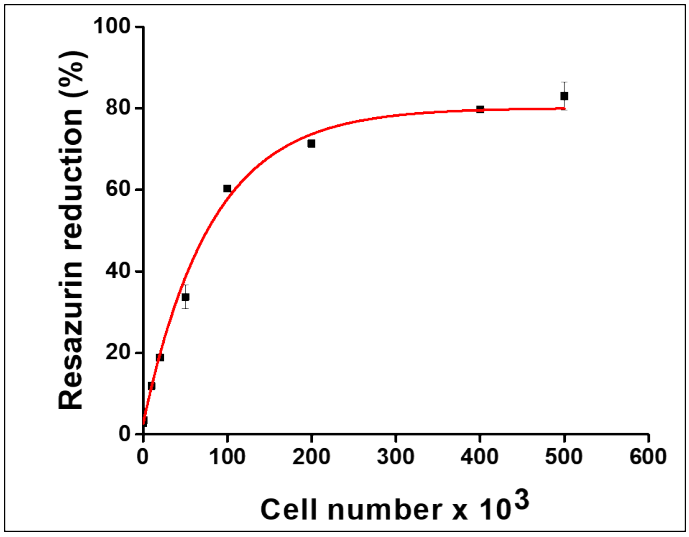

Figure S9. A standard curve of CAD cell number versus percentage of Resazurin reduction.

References

(1) Popinet, S. Gerris: A Tree-Based Adaptive Solver for the Incompressible Euler Equations in Complex Geometries. J. Comput. Phys 2003, 190 (2), 572-600.

(2) Popinet, S. An Accurate Adaptive Solver for Surface-Tension-Driven Interfacial Flows. J. Comput. Phys 2009, 228 (16), 5838-5866.

(3) Afkhami, S.; Bussmann, M. Height Functions for Applying Contact Angles to 2D VOF Simulations. Int. J. Numer. Methods Fluids 2008, 57 (4), 453-472.

(4) Azarmanesh, M.; Farhadi, M.; Azizian, P. Double Emulsion Formation Through Hierarchical Flow-Focusing Microchannel. Phys. Fluids 2016, 28 (3), 032005.

(5) Azarmanesh, M.; Farhadi, M.; Azizian, P. Simulation of the Double Emulsion Formation Through a Hierarchical T-Junction Microchannel. Int. J. Numer. Method. H 2015, 25 (7), 1705-1717.

(6) Azarmanesh, M.; Farhadi, M. The Effect of Weak-Inertia on Droplet Formation Phenomena in T-Junction Microchannel. Meccanica 2016, 51 (4), 819-834.

(7) Chen, X.; Ma, D.; Yang, V.; Popinet, S. High-Fidelity Simulations of Impinging Jet Atomization. At. Sprays s 2013, 23 (12).

(8) Chen, X.; Yang, V. Thickness-Based Adaptive Mesh Refinement Methods for Multi-Phase Flow Simulations with Thin Regions. J. Comput. Phys 2014, 269, 22-39.

(9) Mahady, K.; Afkhami, S.; Kondic, L. A Numerical Approach for the Direct Computation of Flows Including Fluid-Solid Interaction: Modeling Contact Angle, Film Rupture, And Dewetting. Phys. Fluids 2016, 28 (6), 062002.

(10) Fu, J.; Chuah, Y. J.; Ang, W. T.; Zheng, N.; Wang, D.A. Optimization of a Polydopamine (PD)-Based Coating Method and Polydimethylsiloxane (PDMS) Substrates for Improved Mouse Embryonic Stem Cell (ESC) Pluripotency Maintenance and Cardiac Differentiation. Biomater. Sci. 2017, 5 (6), 1156-1173.

(11) Yang, Y.; Qi, P.; Ding, Y.; Maitz, M. F.; Yang, Z.; Tu, Q.; Xiong, K.; Leng, Y.; Huang, N. A Biocompatible and Functional Adhesive Amine-Rich Coating Based on Dopamine Polymerization. J. Mater. Chem. B 2015, 3 (1), 72-81.

(12) Hong, S.; Kim, J.; Na, Y. S.; Park, J.; Kim, S.; Singha, K.; Im, G. I.; Han, D. K.; Kim, W. J.; Lee, H. Poly (Norepinephrine): Ultrasmooth Material-Independent Surface Chemistry and Nanodepot for Nitric Oxide. Angew. Chem. 2013, 52 (35), 9187-9191.

(13) Reddy, S.; Stephan, C. Analysis of Surface Bound Organic Ligands on Gold Nanomaterials Using Direct Sample Analysis–Time of Flight Mass Spectrometry.